Supporting Information

Ternary MnO/CoMn Alloy@N-doped graphitic composites derived from a bi-metallic pigment as bi-functional electrocatalysts

*Chen Deng,[a] Kuang-Hsu Wu,[a] Jason Scott,[a] Shenmin Zhu,[b] Rose Amal[a] and Da-Wei Wang ,[a,c]**

[a]Particles and Catalysis Research Group, School of Chemical Engineering, The University of New South Wales, Sydney, NSW 2052, Australia.

[b]State Key Laboratory of Metal Matrix Composites, School of Materials Science and Engineering, Shanghai Jiao Tong University, Shanghai 200240, China.

[c]UNSW Digital Grid Futures Institute, The University of New South Wales, Sydney, NSW 2052, Australia

Corresponding email: da-wei.wang@unsw.edu.au

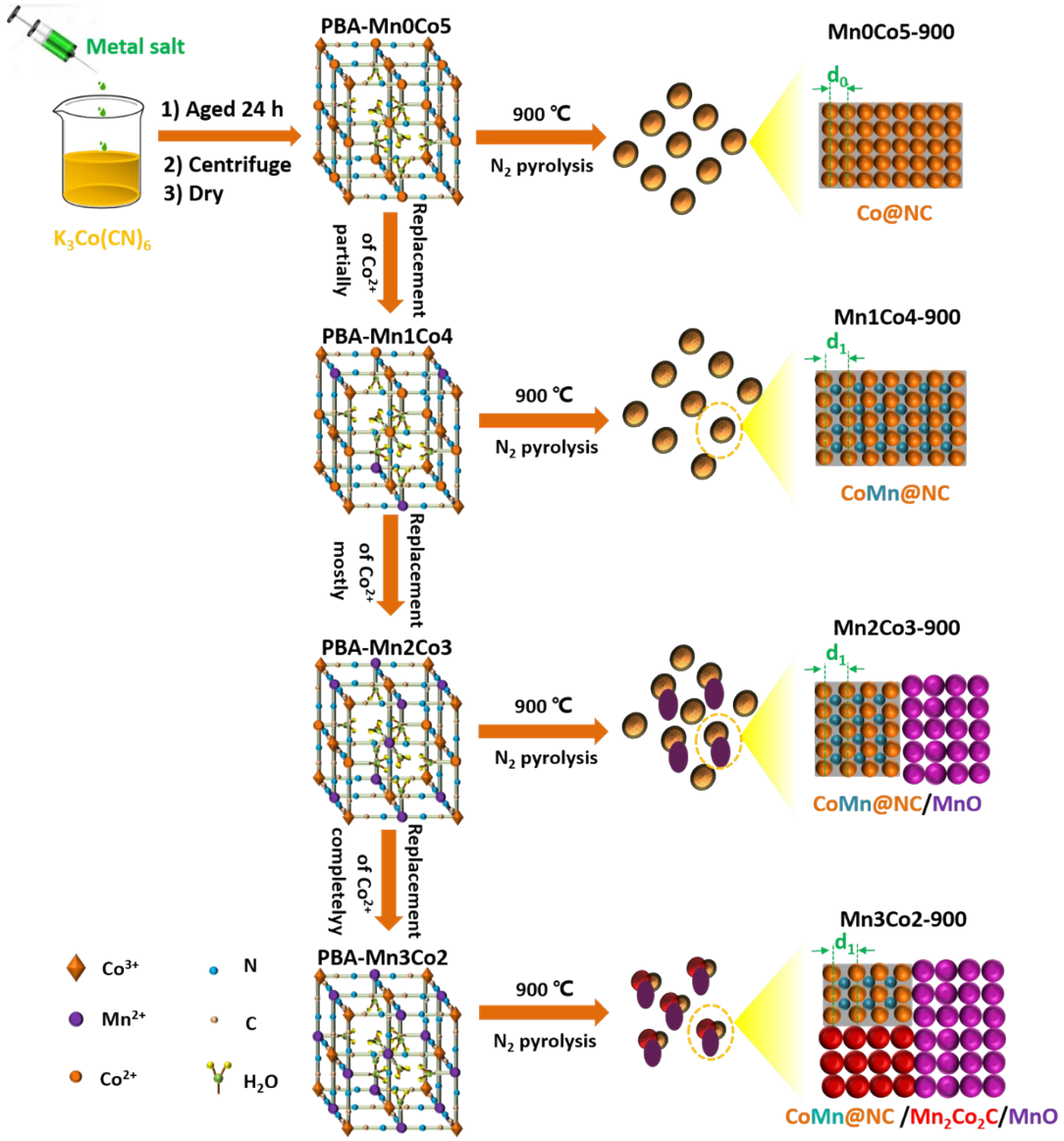

Fig. S1 Schematic detailing the synthesis process for the MnXCoY-900 electrocatalysts.

As illustrated in **Fig. S1**, synthesis of the composite MnXCoY-900 samples comprised a two-step process: (i) preparing the Prussian blue analogues ($M_3[Co(CN)_6]_2$, M=Co^{2+} or Mn^{2+}) by coprecipitation; (ii) annealing the PBA-MnXCoY at 900 °C in a nitrogen atmosphere to give the electrocatalytic material. When preparing the PBAs, the molar ratio of Mn/Co atoms in the structure was controlled by modifying the concentration of cobaltous nitrate and manganese nitrate in the reacting solution. Four samples were prepared with fixed total Mn/Co ratios of 0:5, 1:4, 2:3 and 3:2 (PBA-Mn0Co5, PBA-Mn1Co4, PBA-Mn2Co3 and PBA-Mn3Co2, respectively). Annealing the PBA-MnXCoY precursors can produce MnXCoY-900 materials which was with different make-ups. N and C atoms within the PBA produce a N-doped carbon structure, integrated with the Co/Mn particles upon annealing.

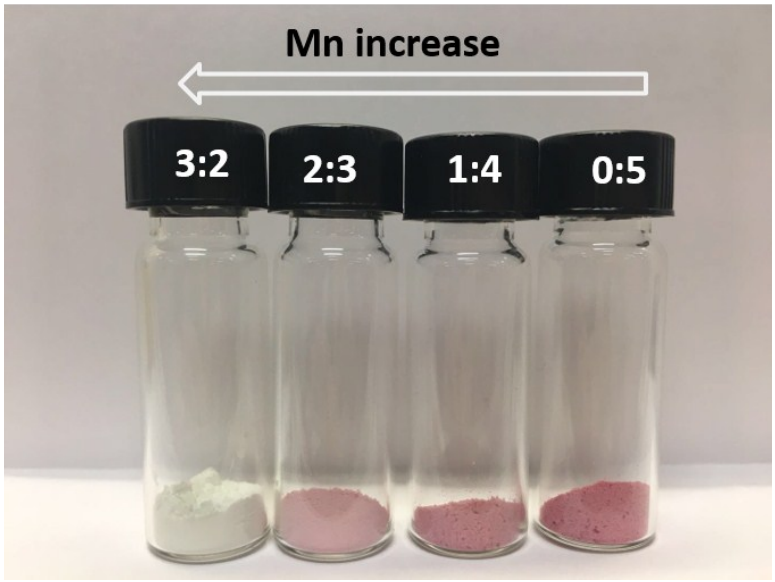

Fig. S2 The colour evolution of PBA precursors with different Mn/Co ratios (3:2, 2:3, 1:4, 0:5).

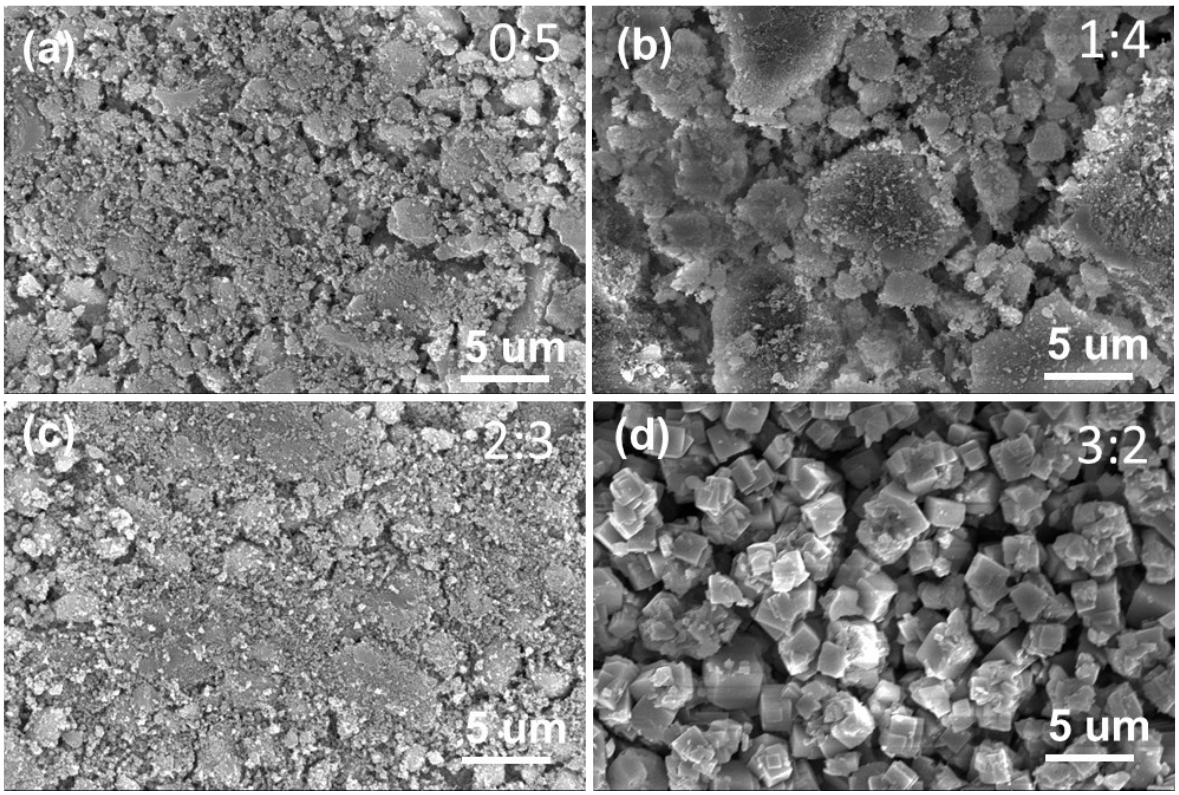

Fig. S3 SEM images of PBA precursors. (a) PBA-Mn0Co5, (b) PBA-Mn1Co4, (c) PBA-Mn2Co3, and (d) PBA-Mn3Co2.

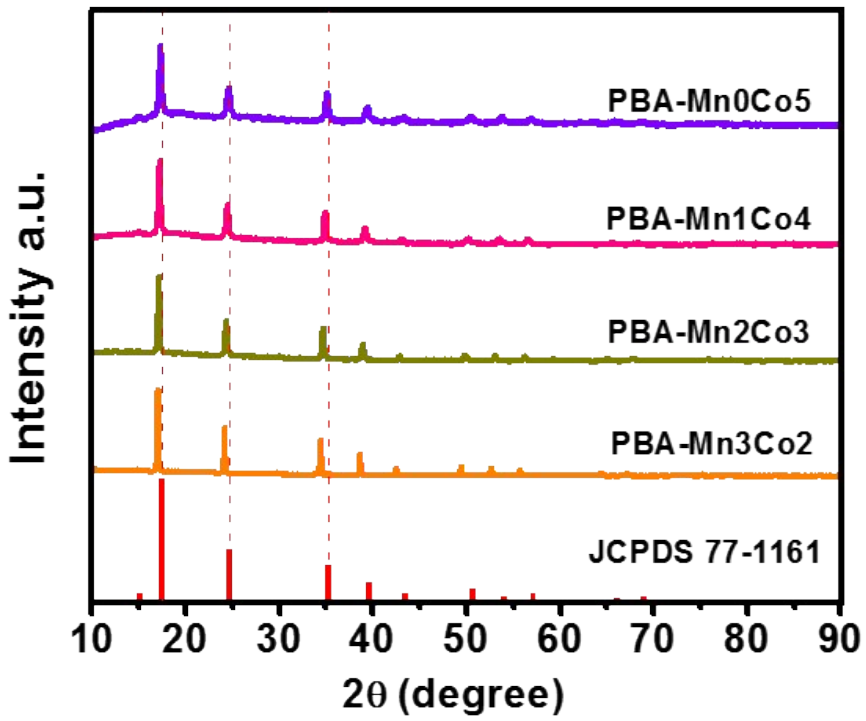

Fig. S4 XRD patterns of PBA precursors with different Mn/Co ratios.

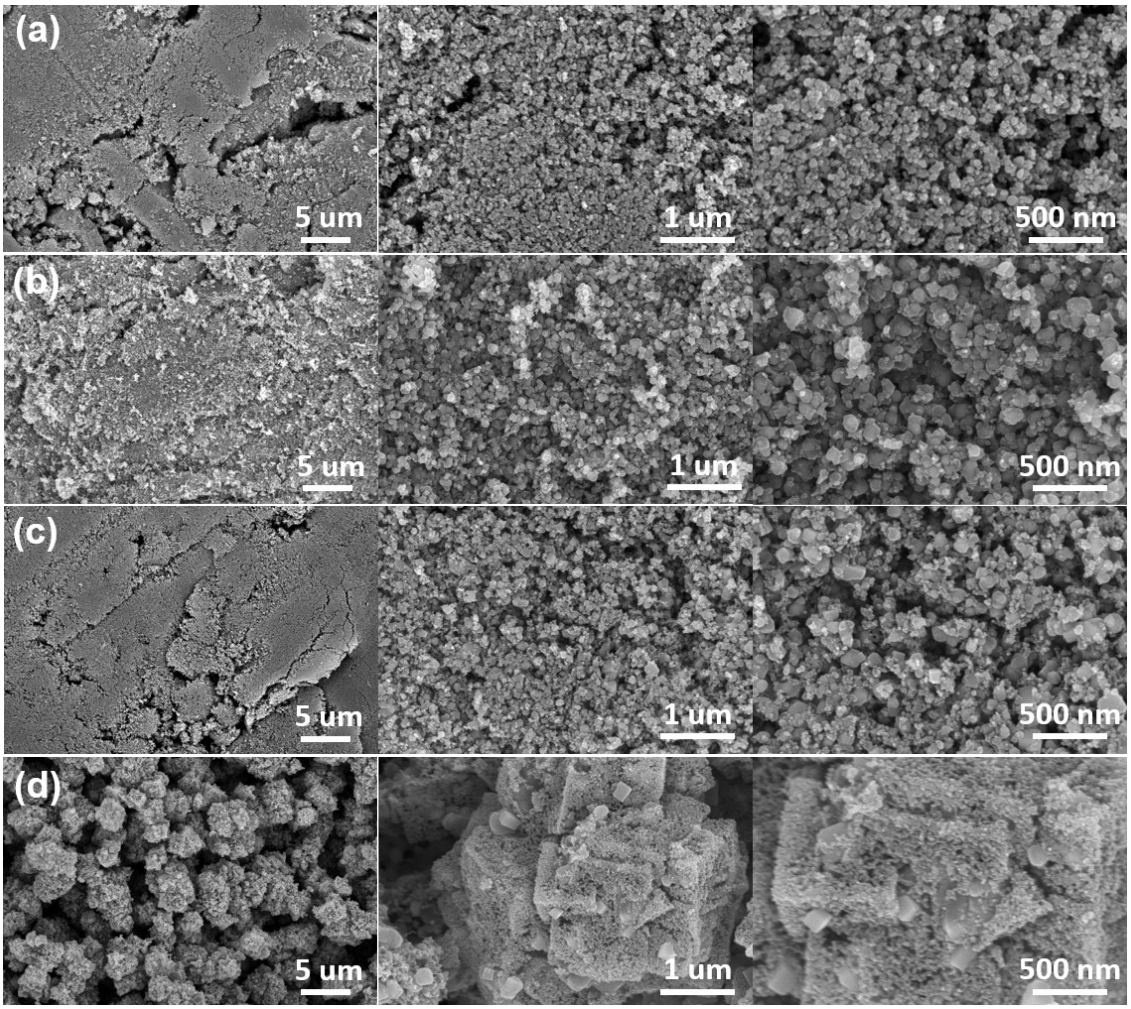

Fig. S5 SEM images of all resultant electrocatalysts with different Mn/Co ratios (a) Mn0Co-900, (b) Mn1Co4-900, (c) Mn2Co3-900, and (d) Mn3Co2-900.

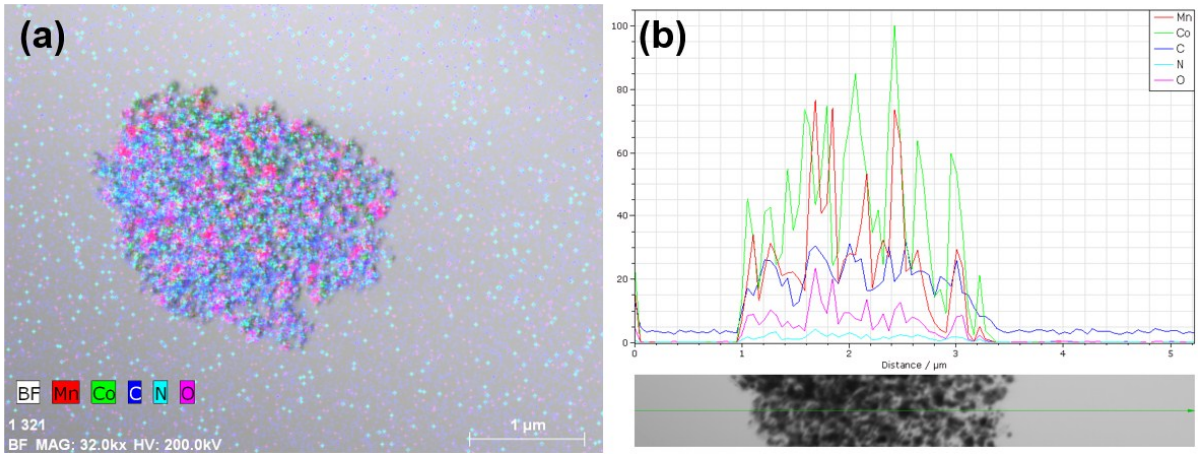

Fig. S6 Overlapped Co, Mn, C, N and O EDX maps for Mn2Co3-900 and a corresponding elemental line scan.

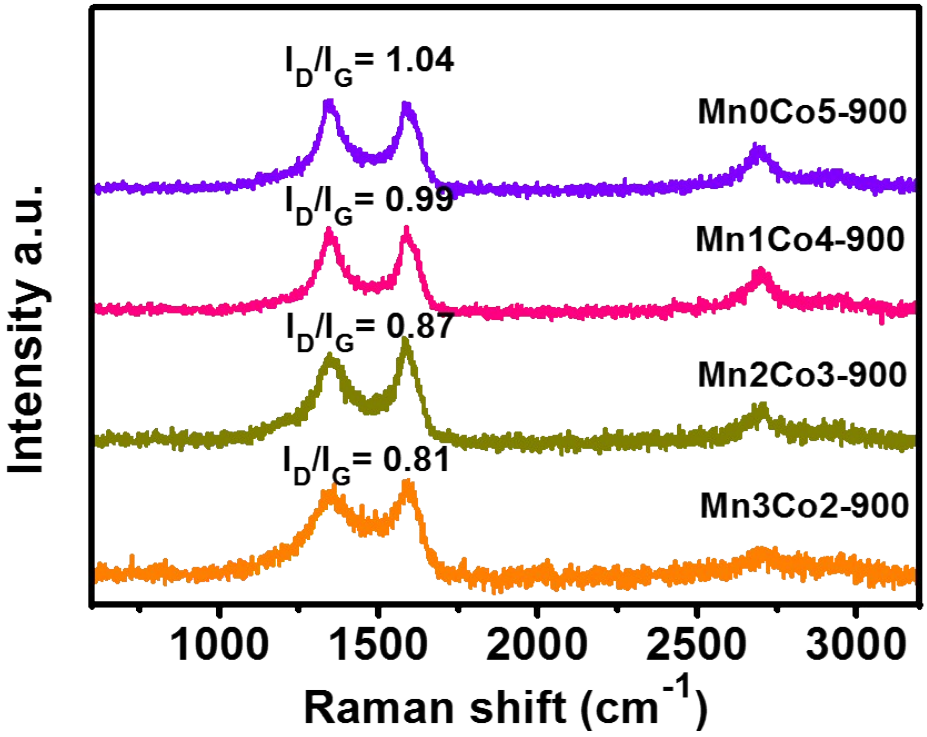

Fig. S7 Raman spectra for Mn0Co-900, Mn1Co4-900, Mn2Co3-900, and Mn3Co2-900.

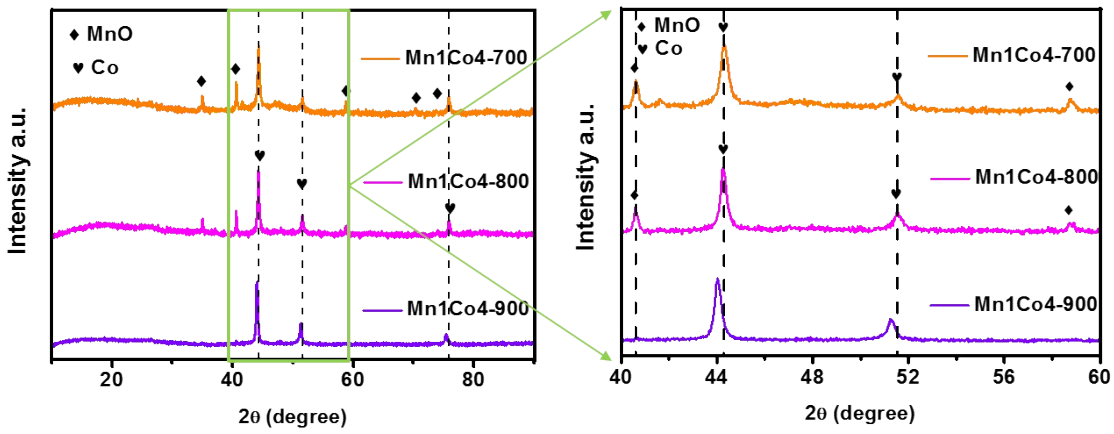

Fig. S8 XRD patterns for Mn1Co4-T (T= 700, 800, 900), and magnification of the selected region within the XRD spectra.

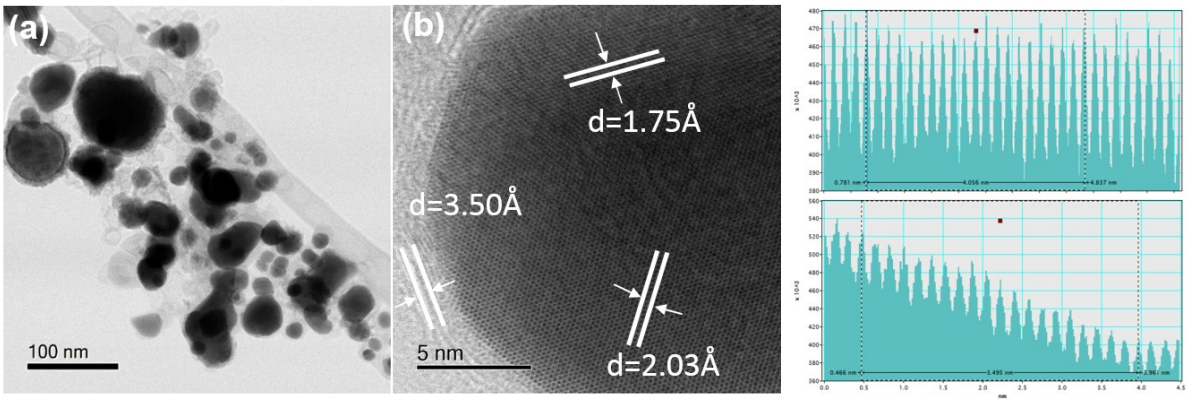

Fig. S9 (a) BF-STEM image of Mn0Co-900; (b) High resolution BF-STEM image of single Mn0Co-900 particle and corresponding lattice spacing.

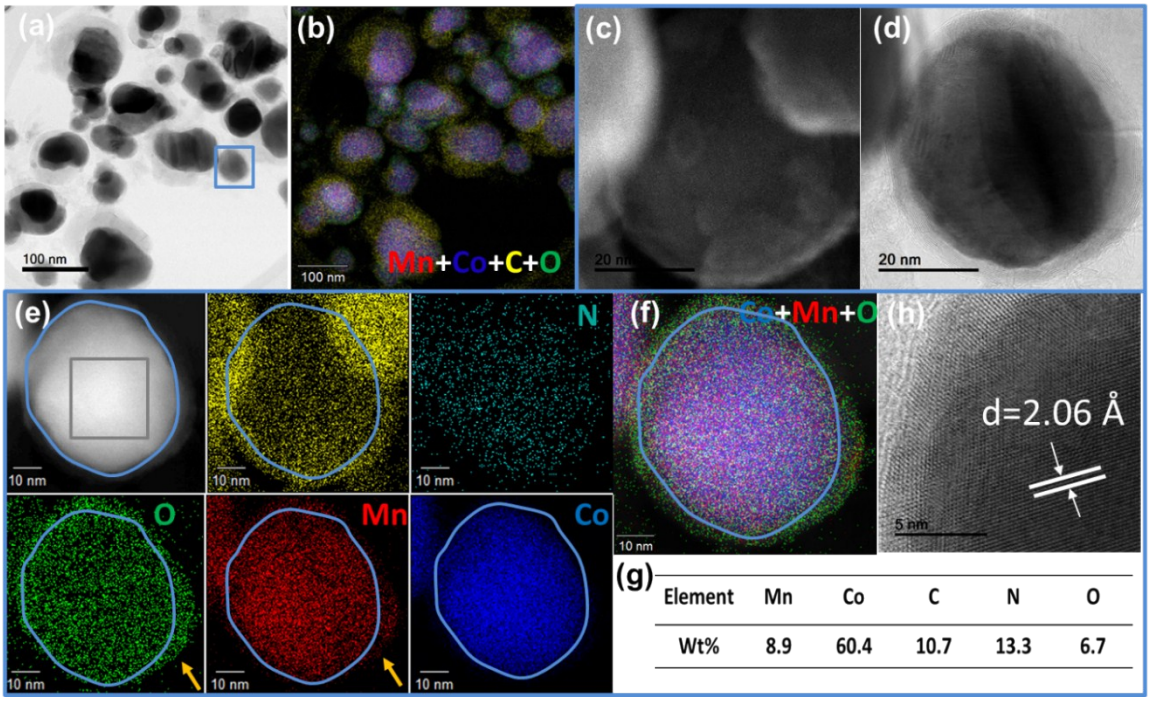

Element	Mn	Co	C	N	O
Wt%	8.9	60.4	10.7	13.3	6.7

Fig. S10 (a) BF-STEM image and (b) HAADF-STEM-EDX mapping of Mn1Co4-900 at low maganification; (c-f) SEM image, BF-STEM image and HAADF-STEM-EDX mapping of single particle in Mn1Co4-900 at high magnification; (g) Percentage amount of each element in selected region (highlighted by grey square) according to HAADF-STEM-EDX mapping; (h) High-resolution BF-STEM image of single particle in Mn1Co4-900 and the corresponding lattice spacing.

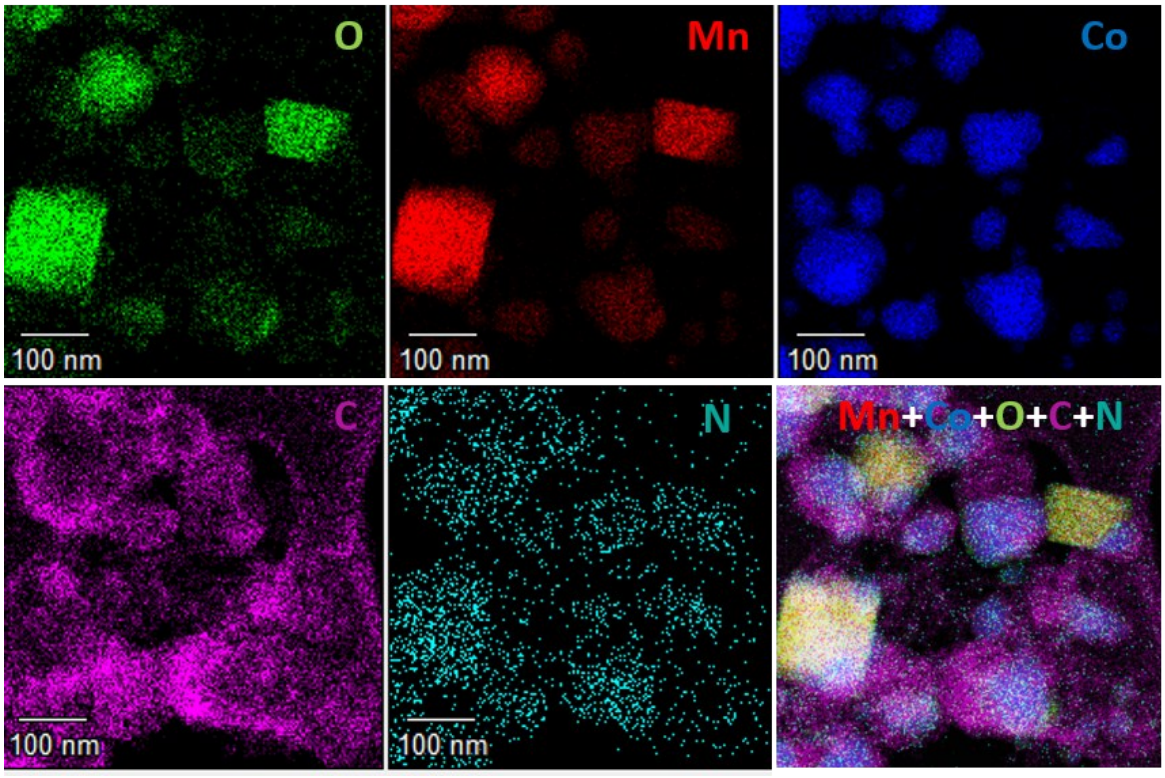

Fig. S11 HAADF-STEM-EDX mapping of Mn2Co3-900 at high maganification.

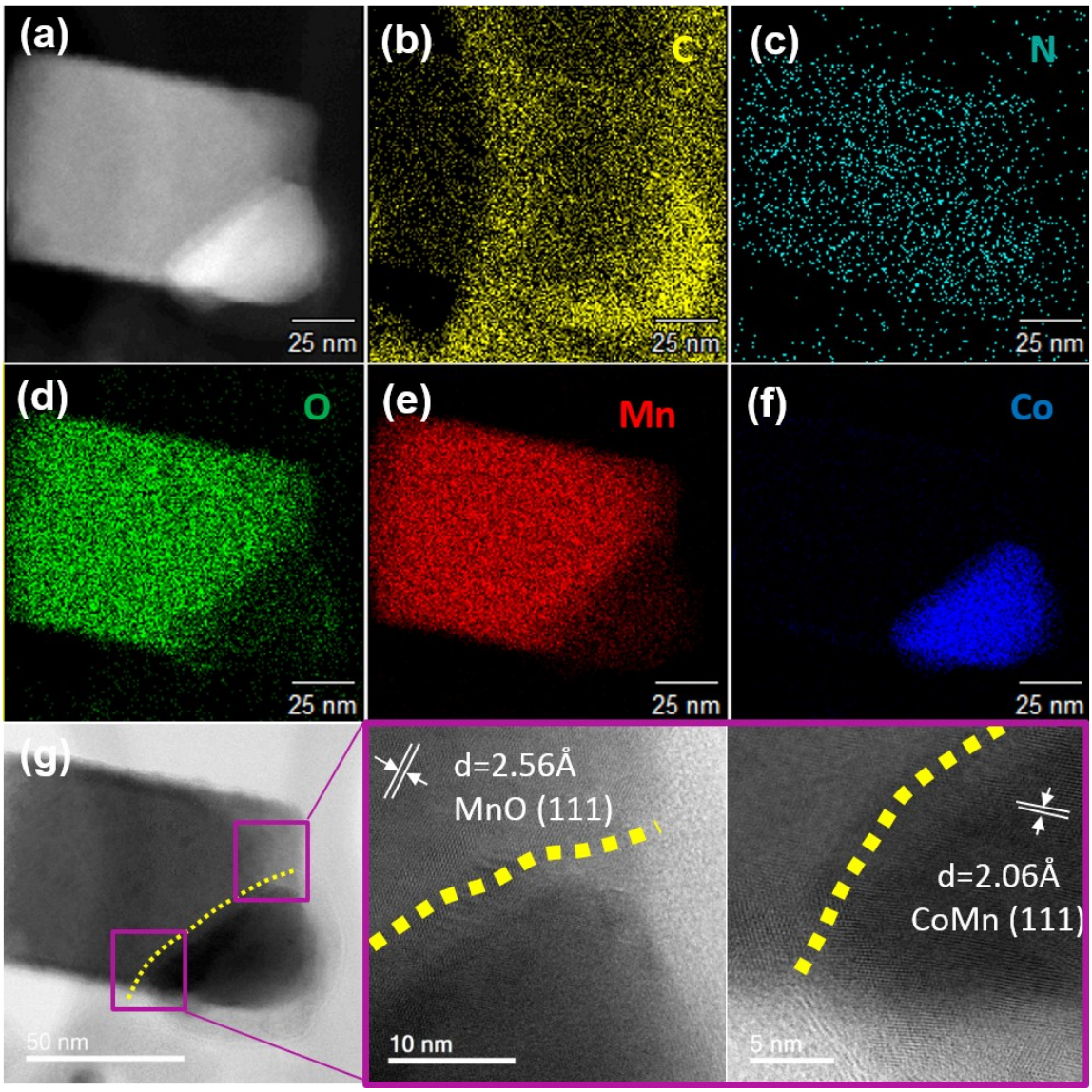

Fig. S12 (a-f) HAADF-STEM-EDX mapping of typical CoMn@CN (containing Co:Mn alloy) particle integrated with MnO in Mn2Co3-900; (g) Corresponding high-resolution BF-STEM images and lattice spacing.

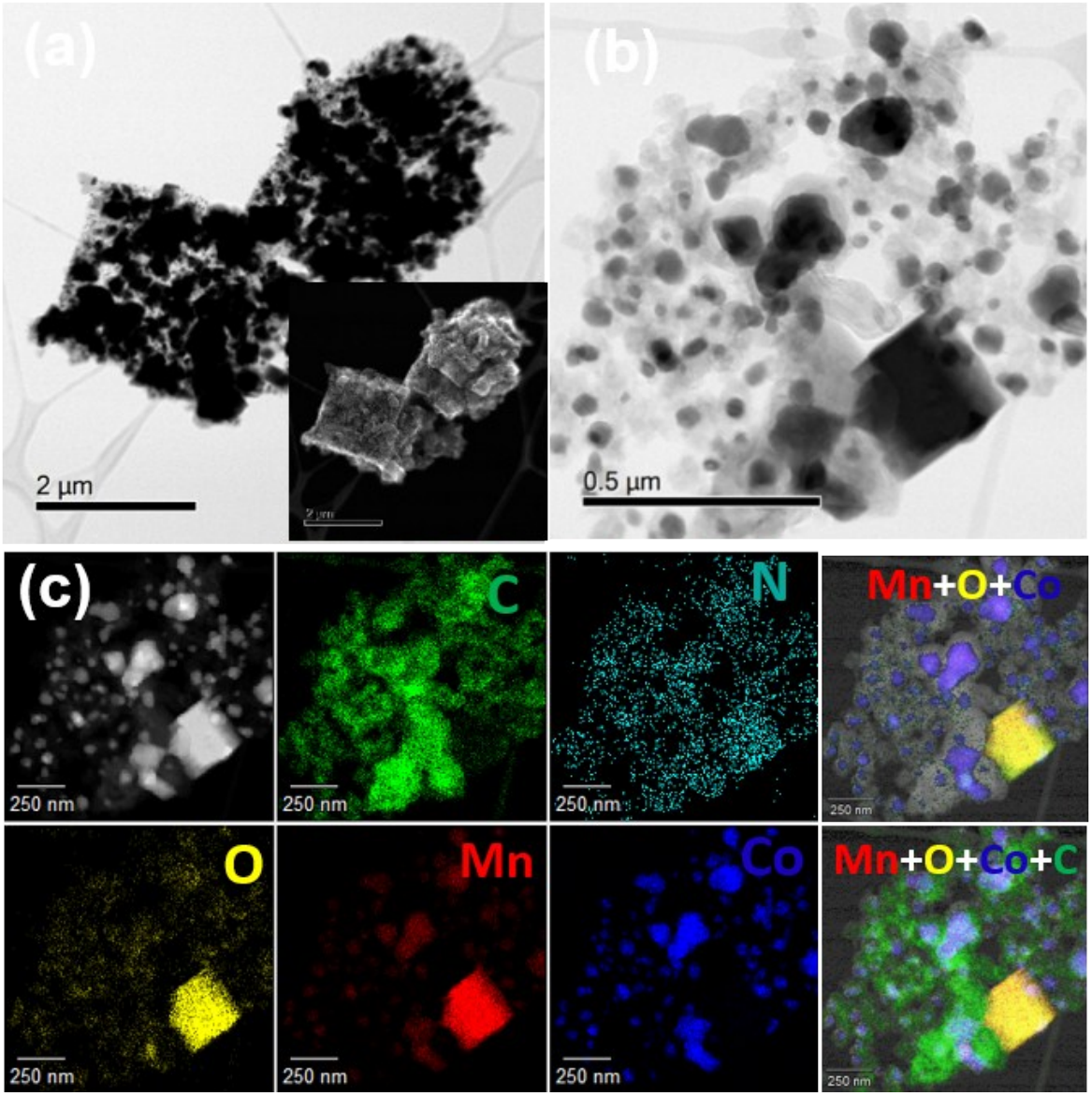

Fig. S13 (a-b) BF-STEM images of Mn3Co2-900 at different maganifications (inset: corresponding SEM image); (c) HAADF-STEM-EDX mapping of Mn3Co2-900.

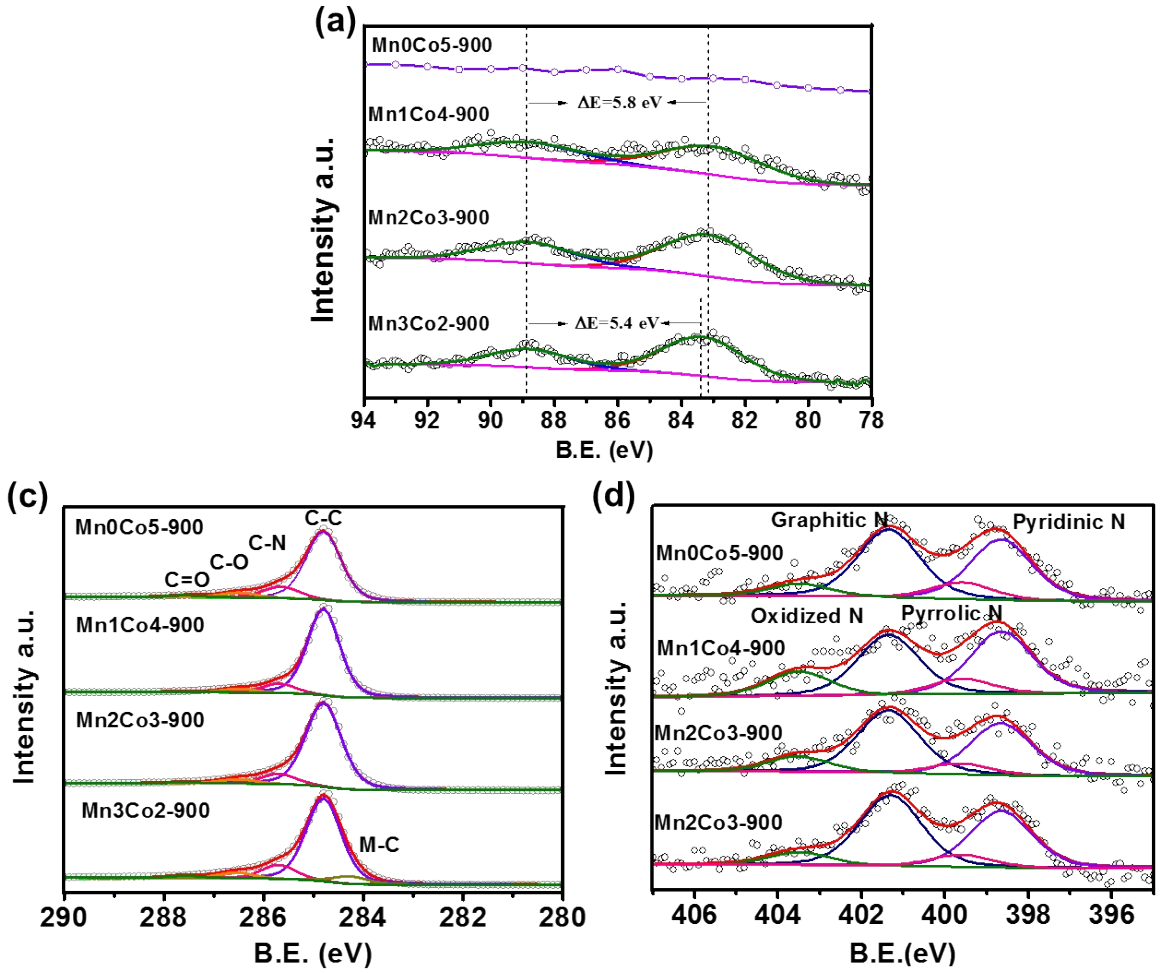

Fig. S14 High resolution XPS spectra of (a) Mn 3s, (b) C1s and (c) N1s regions for Mn0Co-900, Mn1Co4-900, Mn2Co3-900, and Mn3Co2-900.

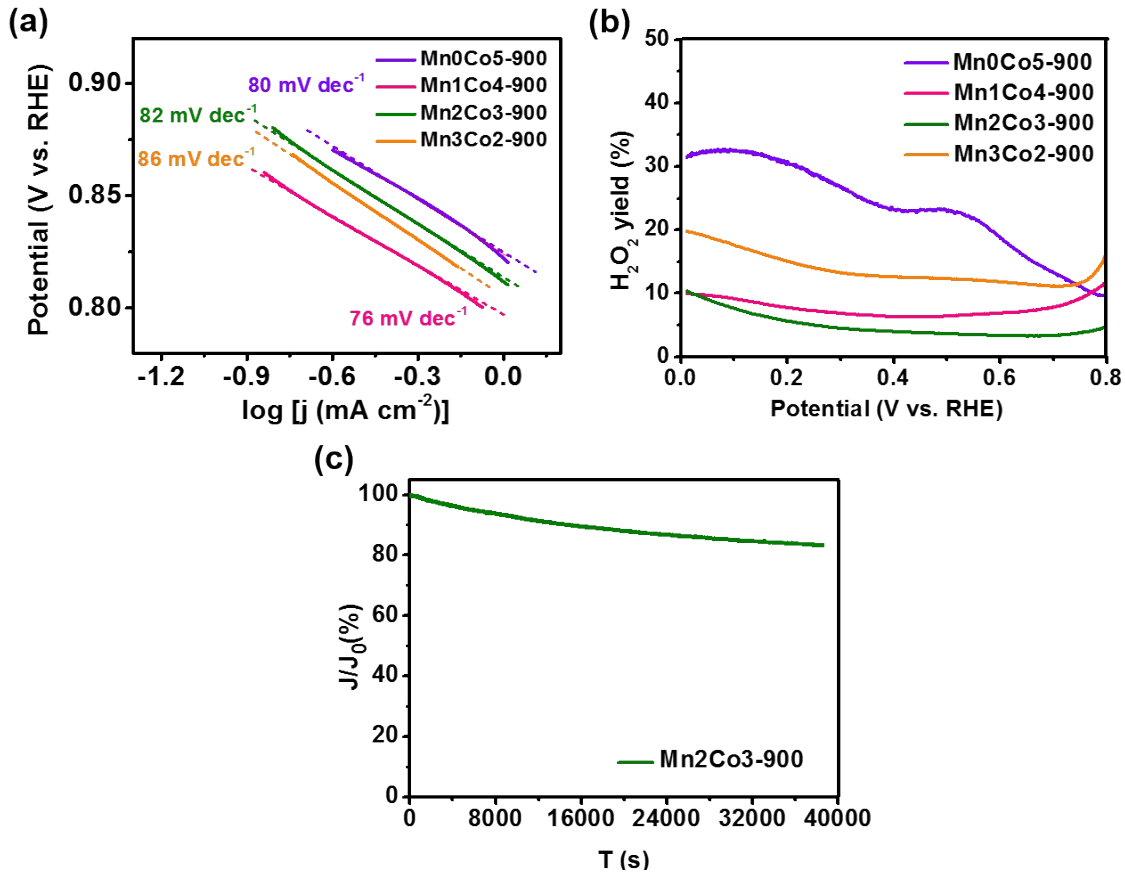

Fig. S15 (a) Tafel plots of Mn0Co-900, Mn1Co4-900, Mn2Co3-900, and Mn3Co2-900 derived from LSV for ORR at high potential range; (b) Hydrogen peroxide yeild by Mn0Co-900, Mn1Co4-900, Mn2Co3-900, and Mn3Co2-900 collected from RRDE analysis during the ORR in O_2 saturated 0.1 M KOH solution at 1600 rpm; (c) chronoamperometry curves of Mn2Co3-900 in O_2-saturated 0.1 M KOH solution at 0.5 V vs RHE for 40000s.

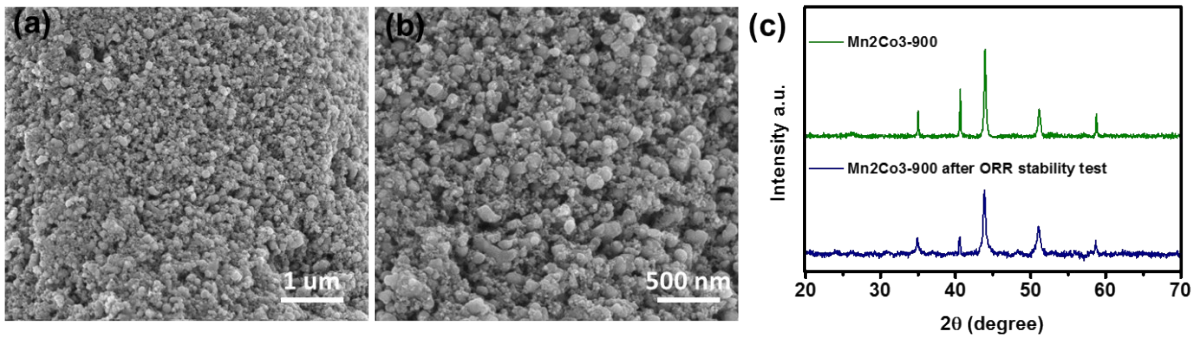

Fig. S16 (a-b) SEM images of Mn2Co3-900 after stability test for ORR at different magnifications; (b) XRD patterns of Mn2Co3-900 before and after ORR stability test.

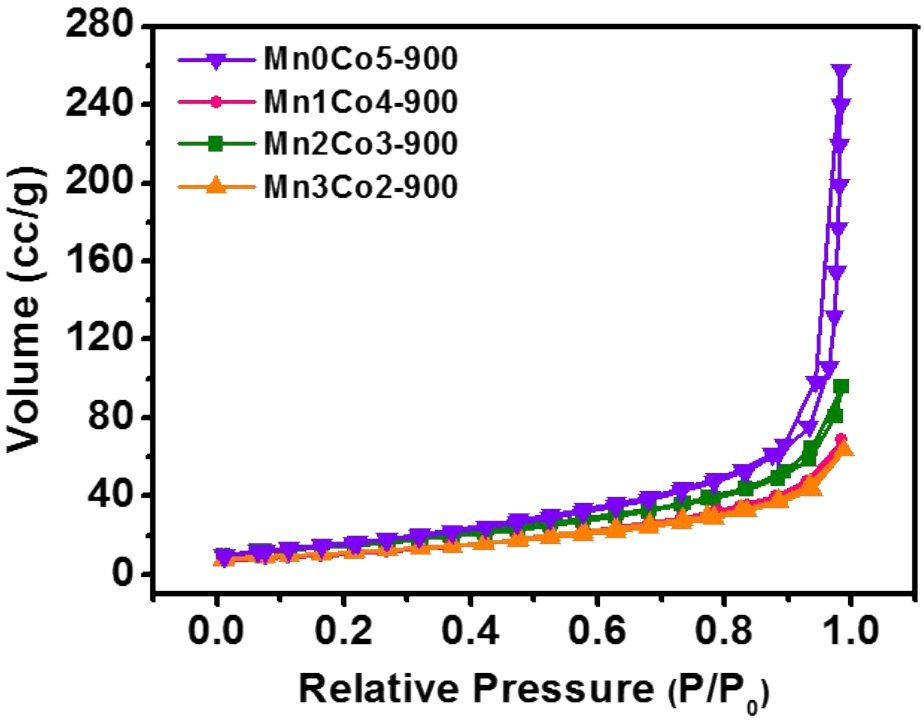

Fig. S17 Nitrogen adsorption-desorption isotherms for Mn0Co-900, Mn1Co4-900, Mn2Co3-900, and Mn3Co2-900.

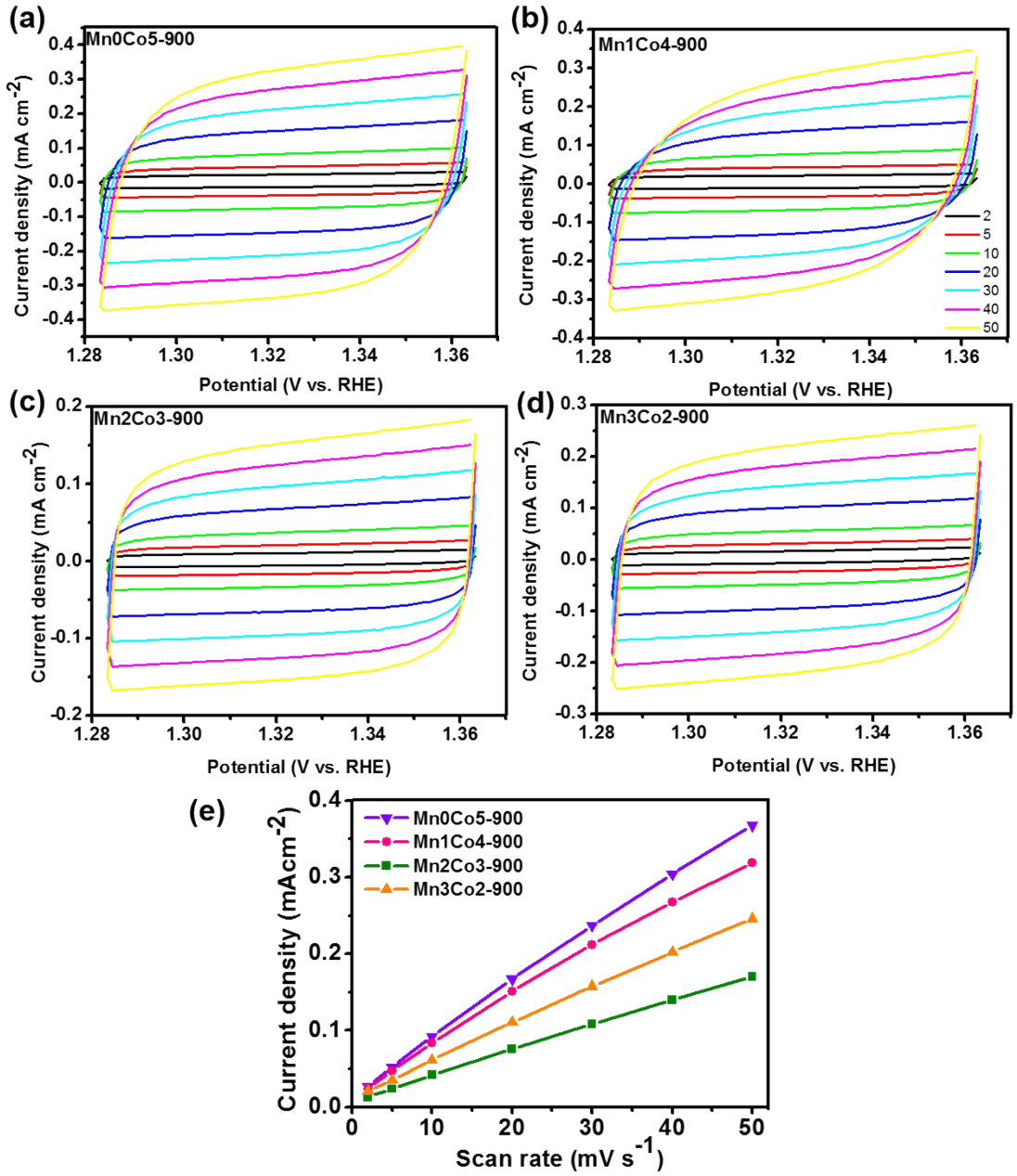

Fig. S18 CV curves within a potential window of 1.28 to1.36 V vs RHE without Faradaic processes at scan rates of 2, 5, 10, 20, 30, 40 and 50 mV s^{-1}: (a) Mn0Co-900; (b) Mn1Co4-900; (c) Mn2Co3-900; and (d) Mn3Co2-900. (e) Current density at 1.34V vs RHE (taken from CV curves) in relation to scan rate.

The electrochemical double layer capacitance (EDLC) of all catalysts was measured within a potential range without Faradaic response to compare the electrochemical active surface area (ECSA) due to the proportional relation between EDLC and ECSA. Typically, a series of CV curves were generated at different scan rates (2, 5, 10, 20, 30, 40, and 50 mV s^{-1}) within a potential range of 1.28–1.36 V. The EDLC was calculated by plotting the different anodic current at 1.34 V against the scan rates. The slope of the linear fitting line represented the EDLC, which indicates the tendency of the ECSA for the resulting catalysts.

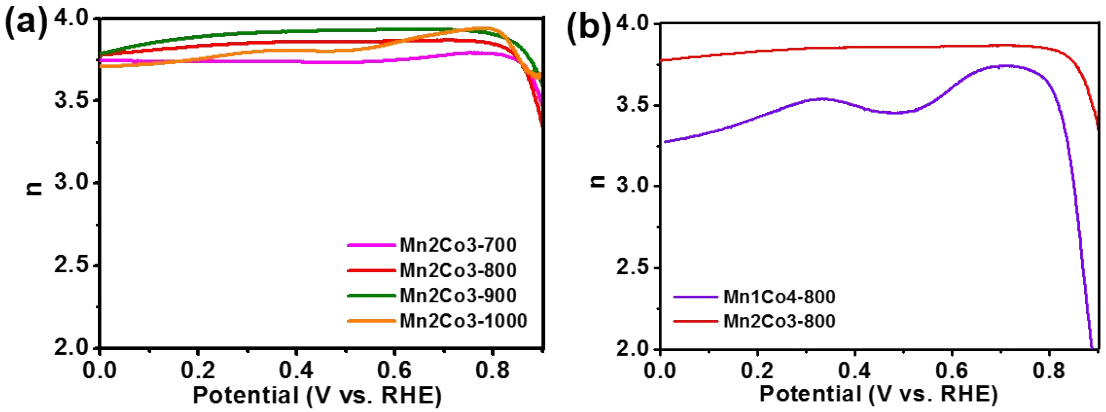

Fig. S19 Electron transfer number of (a) Mn2Co3-T (T=700, 800, 900, 1000) and (b) Mn2Co3-800 and Mn1Co4-800 for the ORR.

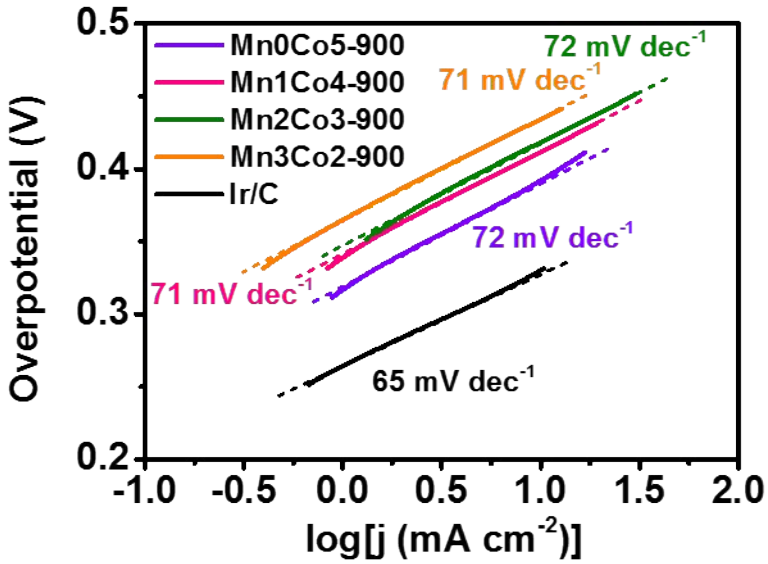

Fig. S20 Tafel plots of Mn0Co-900, Mn1Co4-900, Mn2Co3-900, Mn3Co2-900 and benchmark Ir/C for OER in 1.0 M KOH.

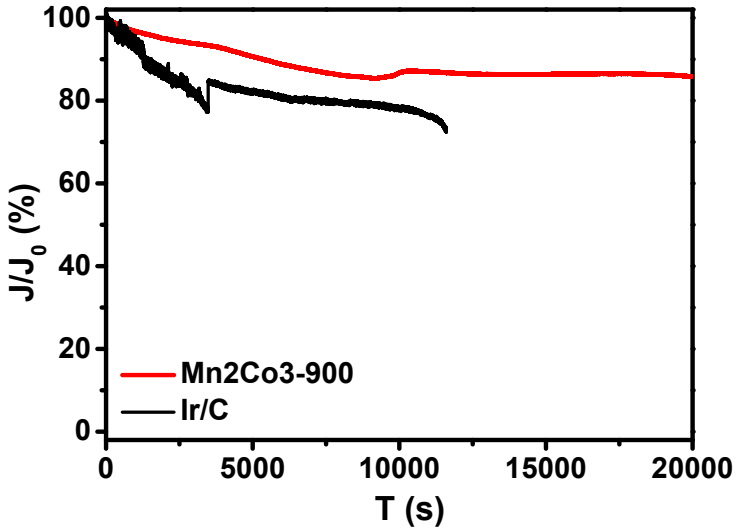

Fig. S21 Chronoamperometry curves of Mn2Co3-900 and Ir/C in 1 M KOH solution at 1.65 V vs. RHE.

Table S1 BET surface area and EDLC values for Mn0Co-900, Mn1Co4-900, Mn2Co3-900, and Mn3Co2-900.

	Mn0Co5-900	Mn1Co4-900	Mn2Co3-900	Mn3Co2-900
BET surface area (m^2/g)	57.7	37.8	52.3	39.9
EDLC (mF cm^{-2})	7.1	6.2	3.3	4.7

Table S2 Comparison of the ORR/OER performance between catalysts prepared in this work and other bifunctional catalysts from the literature.

Catalyst	Loading (mg cm^{-2})	ORR			OER	Ref.
		E_{onset} (V vs. RHE)	$E_{1/2}$ (V vs. RHE)	I* (mA cm^{-2})	$E_{10mA\ cm-2}$ (V vs. RHE)	
MnO/Co/PGC	0.50	0.95	0.78	6	1.54 [a]	1
CoZn-NC-700	0.25	0.98	0.84	4.93	1.63[b]	2
Co_9S_8/CNT	0.2	0.94	0.82	5	1.60 [b]	3
NiFe-LDH/Co,N-CNF	0.12	0.89	0.79	5.1	1.54 [b]	4
FeCo/NPC	0.485	/	0.78	5.3	1.59 [b]	5
PPy/FeTCPP/Co	0.3	1.01	0.86	5.1	1.61 [b]	6
Co@Co_3O_4 /NC-1	0.21	/	0.8	5.1	1.65 [b]	7
PCN-CFP	0.2	0.94	0.67	/	1.63 [b]	8

N, P, and F tri-doped Graphene	0.5	0.9	0.76	5.5	1.8 [b]	9
ZnCo-PVP-900	0.28	0.92	0.83	5.3	1.63[a]	10
Mn0Co5-900	0.28	0.92	/	/	1.62 [a]	This work
Mn1Co4-900	0.28	0.89	0.73	4.1	1.64 [a]	
Mn2Co3-900	0.28	0.91	0.76	5.8	1.65 [a]	
Mn3Co2-900	0.28	0.90	0.75	4.8	1.66 [a]	
Pt/C	0.28	0.95	0.83	5.4	/	
Ir/C	0.28	/	/	/	1.56 [a]	

I* represents the limiting current density obtained at a rotation speed of 1600 rpm in RDE or RRDE.
[a] presents the electrolyte for OER is 1M KOH; while [b] is 0.1 M KOH.

References:

1 X. F. Lu, Y. Chen, S. Wang, S. Gao and X. W. (David) Lou, *Adv. Mater.*, 2019, **31** 1902339.

2 B. Chen, X. He, F. Yin, H. Wang, D.-J. Liu, R. Shi, J. Chen and H. Yin, *Adv. Funct. Mater.*, 2017, **27**, 1700795.

3 H. Li, Z. Guo and X. Wang, *J. Mater. Chem. A*, 2017, **5**, 21353–21361.

4 Q. Wang, L. Shang, R. Shi, X. Zhang, Y. Zhao, G. I. N. Waterhouse, L.-Z. Wu, C.-H. Tung and T. Zhang, *Adv. Energy Mater.*, 2017, **7**, 1700467.

5 H.-X. Zhong, J. Wang, Q. Zhang, F. Meng, D. Bao, T. Liu, X.-Y. Yang, Z.-W. Chang, J.-M. Yan and X.-B. Zhang, *Adv. Sustain. Syst.*, 2017, **1**, 1700020.

6 J. Yang, X. Wang, B. Li, L. Ma, L. Shi, Y. Xiong and H. Xu, *Adv. Funct. Mater.*, 2017, **27**, 1606497.

7 A. Aijaz, J. Masa, C. Rosler, W. Xia, P. Weide, A. J. R. Botz, R. A. Fischer, W. Schuhmann and M. Muhler, *Angew. Chemie Int. Ed.*, 2016, **55**, 4087–4091.

8 T. Y. Ma, J. Ran, S. Dai, M. Jaroniec and S. Z. Qiao, *Angew. Chemie Int. Ed.*, 2015, **54**, 4646–4650.

9 J. Zhang and L. Dai, *Angew. Chemie Int. Ed.*, 2016, **55**, 13296–13300.

10 C. Deng, K.-H. Wu, J. Scott, S. Zhu, X. Zheng, R. Amal and D.-W. Wang, *ACS Appl. Mater. Interfaces*, 2019, **11**, 9925–9933